Lab on a Chip

PAPER

View Article Online
View Journal



Cite this: DOI: 10.1039/c5lc01027f

# A microchannel device tailored to laser axotomy and long-term microelectrode array electrophysiology of functional regeneration†‡

Rouhollah Habibey,[a] Asiyeh Golabchi,[a] Shahrzad Latifi,[ab] Francesco Difato*[a] and Axel Blau*[a]

We designed a miniaturized and thin polydimethylsiloxane (PDMS) microchannel device compatible with commercial microelectrode array (MEA) chips. It was optimized for selective axonal ablation by laser microdissection (LMD) to investigate the electrophysiological and morphological responses to a focal injury in distinct network compartments over 45 days *in vitro* (45 DIV). Low-density cortical or hippocampal networks (<3500 neurons per device) were cultured in quasi-closed somal chambers. Their axons were selectively filtered through neurite cavities and guided into the PDMS microchannels aligned over the recording electrodes. The device geometries amplified extracellularly recorded signals in the somal reservoir and the axonal microchannels to detectable levels. Locally extended areas along the microchannel, so-called working stations, forced axonal bundles to branch out and thereby allowed for their repeatable and controllable local, partial or complete dissections. Proximal and distal changes in the activity and morphology of the dissected axons were monitored and compared to those of their parent networks and of intact axons in the control microchannels. Microscopy images confirmed progressive anterograde degeneration of distal axonal segments over four weeks after surgery. Dissection on cortical and hippocampal axons revealed different cell type- and age-dependent network responses. At 17 DIV, network activity increased in both the somal and proximal microchannel compartments of the dissected hippocampal or cortical axons. At later days (24 DIV), the hippocampal networks were more susceptible to axonal injury. While their activity decreased, that in the cortical cultures actually increased. Subsequent partial dissections of the same axonal bundles led to a stepwise activity reduction in the distal hippocampal or cortical axonal fragments. We anticipate that the MEA-PDMS microchannel device for the combined morphological and electrophysiological study of axonal de- and regeneration can be easily merged with other experimental paradigms like molecular or pharmacological screening studies.

Received 27th August 2015,
Accepted 15th October 2015

DOI: 10.1039/c5lc01027f

www.rsc.org/loc



## Introduction

Axonal projections are critical for the long-range communication between neuronal subpopulations in both the central and peripheral nervous system (CNS and PNS).[1] Dysfunction and degradation of axonal tissues are early hallmarks of most neurodegenerative disorders. Axonal degeneration follows traumatic injury *in vivo*, which leads to a process known as Wallerian degeneration.[2] To overcome the complexity of monitoring subsequent cellular and molecular events in an entire organism, a few *in vitro* models of axonal injury have been suggested.[3]

Classic *in vitro* axonal injury models include axonal transection by fine glass capillaries, sharp metal blades or glass microelectrodes.[4] However, they are less suited for selective axonal injury in neuronal networks with complex structures and activity profiles as *in vivo* systems. This shortcoming was overcome by optical techniques. Among them are the use of femtosecond near-infrared[5] and nano- to picosecond pulsed lasers.[6–9] In a recent *in vitro* model, Kim *et al.* combined a laser microdissection (LMD) setup with microfluidics to perform more localized and reproducible axotomy.[10]

[a] *Department of Neuroscience and Brain Technologies (NBT), Italian Institute of Technology (IIT), via Morego 30, 16163 Genoa, Italy. E-mail: axel.blau@iit.it, francesco.difato@iit.it*

[b] *Department of Neurology, David Geffen School of Medicine at UCLA, 635 Charles E. Young Dr. South, Los Angeles, CA 90095, USA*

† R. H. designed and implemented the PDMS devices, acquired and analysed the electrophysiological data and wrote the manuscript; A. G. assisted in the device fabrication and the electrophysiology experiments; S. L. assisted in the image acquisition and immunohistochemistry experiments; A. B. initiated the research line and conceived the microchannel experiments; F. D. conceived the LMD experiments; A. B. and F. D. supervised the study. All authors edited the manuscript and gave final approval for its publication.

‡ Electronic supplementary information (ESI) available. See DOI: 10.1039/c5lc01027f

Microfluidic platforms are suitable *in vitro* tools to separate axonal physiology and pathology from that of their cell bodies.[11] For instance, regeneration was studied on isolated axons in microchannels after axotomy by vacuum aspiration.[12,13] However, because this procedure removed the distal axonal compartments, it was not possible to study anterograde or Wallerian degeneration, an important aspect of *in vivo* axonal disintegration. This limitation could be overcome either by picosecond pulsed laser dissection or by mass axotomy using detergent applied through an extra compartment in a modified microfluidic platform.[14,15] Although these models were suitable for studying the molecular biology of degenerating and regenerating axons *in vitro*, axonal electrophysiology and functional network response to an injury have been neglected in almost all recent studies.

The electrophysiology of developing neuronal networks can be monitored over weeks by seeding neurons on multi- or micro-electrode arrays (MEAs) with non-invasive, substrate-integrated planar electrodes.[16] However, in random MEA cultures, most of the network activity is inaccessible because the few electrodes ($<60$) can capture only the activity from neurons placed nearby.[17] More importantly, the amplitudes of the electrophysiological signals in axonal projections are either too low to be detected by extracellular probes or obscured by stronger signals recorded from cell bodies.[18] Therefore, a few laboratories started to combine polydimethylsiloxane (PDMS) microfluidic devices with MEAs to either confine neurons to the electrode areas[18,19] or to guide axons through microchannels aligned with the MEA electrodes to amplify and record axonal activity.[20–22] However, most of these PDMS devices were developed for custom-made rather than commercial MEAs and are therefore not available in other laboratories.[18,23,24]

In the present study, we developed a miniaturized PDMS microchannel device and a simple cell loading protocol adaptable to most commercial MEAs with different medium-retaining ring diameters. We defined and met several optimization criteria for combining an independent and versatile axonal microchannel confinement module with LMD[25] and MEA electrophysiology for selective axonal transection and long-term follow-up imaging and activity studies.

# Methods

### PDMS microchannel device fabrication

A two-layer SU-8 template was fabricated on a polished 4″ silicon wafer (Si-Mat). The silicon substrates were subsequently spin-coated with SU-8 5 and SU-8 50 (MicroChem) to generate two patterned layers of different heights (5 μm for the microchannels and 100 μm for the reservoirs). The SU-8 layer thickness was controlled by the spinning speed (Ws-650Sz Spin Coater, Laurell Technologies). Each SU-8 layer was photopatterned in a mask aligner (MJB4, SUSS MicroTec) with separate chrome (Photronics Ltd.) or printed high-definition transparency masks (Repro S.r.l.) to form SU-8 stripes and reservoirs. Pre-, post- and hard-bake as well as SU-8 development protocols were followed as suggested in the product datasheets. The thicknesses and widths of the final structures were determined by using a stylus profiler (Wyko NT1100, Veeco) and quantitative microscopy (Leica DM IL LED Inverted, Leica Microsystems CMS Gmbh) through Zeiss Axiovision software (version 4.8) measurements.

Each device included 8 microchannels ($w$ = 30 μm, $l$ = 800 μm, $h$ = 5 μm), two neurite filter areas ($w$ = 100 μm, $l$ = 1500 μm, $h$ = 5 μm), two somal reservoirs ($w$ = 400 μm, $l$ = 1600 μm, $h$ = 100 μm) and four seeding cavities ($r$ = 1 mm, $h$ = 200 μm). We designed three wider, diode-shaped areas ($w$ = 60 μm, $l$ = 60 μm), so-called 'working stations', along three out of 8 microchannels, which were later utilized for axonal branching and microdissection. Therefore, each device featured five classic microchannels (μ-ch) and three microchannels with working stations (μ-ch_ws). A neurite filter cavity separated the reservoirs from the microchannels on each side to prevent the dendrites and cell bodies from invading the microchannel entrance.

PDMS microchannel tiles were fabricated by soft lithography. PDMS (Sylgard 184, Dow Corning) pre-polymer and curing agent were mixed (10 : 1), degassed and poured on either the original SU-8 template or an epoxy copy thereof (Epox A cast 655, Smooth-On). PDMS was levelled to the highest topographies by squeezing it out of the cavities with the help of a laser copier transparency. To provide closed somal reservoirs in place of open reservoirs, a very thin layer of PDMS was left between the transparency and the template's highest structures. PDMS was cured at room temperature for 48 hours or at 80 °C for 25 min. After peeling the thin PDMS device from the patterned template, four big seeding cavities were manually punched with a puncher at the two opposite outer corners of each small somal reservoir. The final device thus featured four big round-shaped seeding cavities with openings from the top and two junctional quasi-closed somal reservoirs, which were connected through the 8 microchannels. The individual steps and device features are depicted in Fig. 1.

### Alignment and cell seeding

The PDMS microchannel tiles were baked in an oven at 100 °C for 24 hours to finalize the cross-linking of uncured oligomers and dry-autoclaved at 120 °C for 20 minutes before being moved to the sterile hood. Then, a device was manually aligned with the 60 MEA electrodes (30/200 i.r., Multi Channel Systems) under a microscope (5× magnification) to place four electrodes in each microchannel and 14 electrodes in each somal reservoir. The wider areas of the microchannels with working stations (μ-ch_ws) were aligned between the electrodes to optically cut axons without damaging the electrodes or connecting wires. A droplet of ultrapure water (MilliQ, MQ) or ethanol (96%) was used to facilitate the alignment procedure. Both the PDMS device and the exposed MEA surfaces were hydrophilized by oxygen plasma (2–3 min, 60 W, 2.45 GHz, 0.4 mbar $O_2$) (femto, Diener). PDMS devices were

 

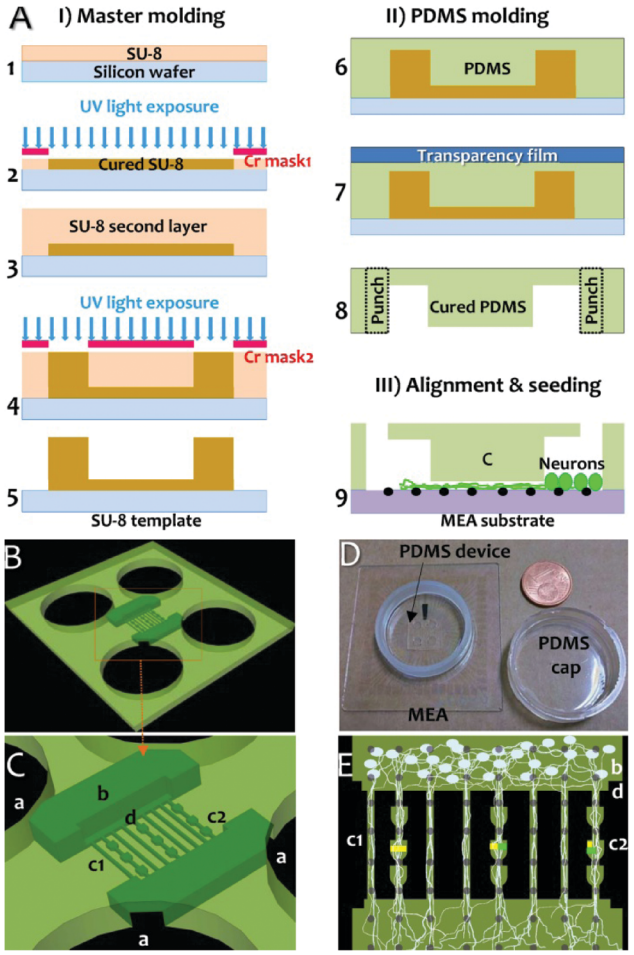


**Fig. 1** Master molding, PDMS device fabrication, alignment and cell seeding. A) SU-8 template fabrication in five steps (I), PDMS microdevice molding in three steps (II), and side view of the aligned PDMS device on MEA electrodes (black disks) and of growing axons inside the microchannels (III). B) PDMS device with four big cell seeding pools. C) Magnified view of punched pools (a), closed somal reservoir (b), classic microchannels (μ-ch, c1), microchannels with working stations (μ-ch_ws, c2), and neurite filtering cavity (d). D) Aligned PDMS device on MEA and a PDMS cap for sealing the culture against evaporation and contamination. E) Top view sketch of C with a network inside the aligned PDMS device. Yellow marks denote complete, partial or local dissections at 17 DIV, and green marks denote partial dissections at 24 DIV. Electrodes are represented by gray disks. In each microchannel, 2 electrodes recorded from proximal axons and the subsequent 2 electrodes from distal axons.

also placed on cover slips for control and histochemistry studies. Subsequently, the MEA or coverslip surface was coated with 5 μl of a 0.1 mg $ml^{-1}$ poly-D-lysine (PDL) and 0.05 mg $ml^{-1}$ laminin mixture in MQ water. The drop was added through one open seeding cavity and was allowed to spread on the surface of the closed chambers and the microchannels. The coating was dried in a vacuum chamber for one minute. The whole device was then submerged three times in MQ water for 10 min each. To remove air bubbles, the device was rinsed with MQ water and vacuumed for a few seconds. The MQ water in the microchannels was replaced with cell culture medium or PBS (1%) by diffusion during overnight incubation (5% $CO_2$, 37 °C, 95% RH). The cell culture medium or PBS was drained from the device and rat cortical or hippocampal neurons (6000 cells per μl) were added through one of the large seeding cavities; they automatically entered and settled in the small somal reservoir on top of a subset of electrodes. The cells distributed homogenously in this somal reservoir with a maximum number of 3500 cells per device. After incubating for five minutes in the incubator, non-adherent cells were removed from the seeding cavities and 1.5 ml of prewarmed serum-free cell culture medium (Neurobasal medium, B27 2%, Glutamax 1%, penicillin/streptomycin 1%) was added to each MEA or coverslip in a 12-well plate. The MEA ring was then sealed with a custom-made gas-permeable PDMS cap[26] before the MEA device assembly was placed in a plastic Petri dish and returned to the incubator. The well-plates were sealed with Parafilm. The cells were kept inside the incubator over the entire duration of the study except for partial medium-exchange (≤50%), recording, microscopy and dissection. The recording, microscopy, and culture medium-exchange days are given in Table 1.

### Electrophysiology

The network activity was recorded using a commercially available 60-channel MEA filter-amplifier (0.1 Hz–25 kHz, 1200× amplification, MEA1060-upright-standard) with an A/D conversion card (64-channels, 25 kHz sampling frequency per channel, PCIbus) and a software user interface (MC_Rack) (all Micro Channel Systems, MCS). Recordings started at 10 DIV. The activity of each culture was acquired daily (up to 45 DIV) for 15 minutes. On the dissection days, the activity was recorded three times from each culture to collect the baseline activity, the activity just after a dissection and three to five hours after a dissection, respectively. During these recordings, the temperature was kept at 37 °C using a built-in thermal sensor and heating element controlled by an external temperature controller (HC-1, MCS). Raw signals were filtered by a second-order Bessel high-pass filter (cut-off at 200 Hz) and analyzed offline. Spikes were detected in the filtered data streams by passing a negative threshold set to −4.5 StDev of the peak-to-peak noise. Spike trains were transformed to time stamps (NeuroExplorer, Nex Technologies); the mean spike frequency on each electrode was extracted as spikes per second.

### Laser microdissection

The LMD setup was described earlier.[27] Briefly, a picosecond pulsed laser (Teem Photonics, PNV-001525-040, 355 nm) was used for dissection with an average power of 10 : 25 μW at the sample and a pulse repetition rate of 100 Hz. The laser was integrated in an inverted Nikon Eclipse Ti microscope featuring a motorized stage, an ergonomic controller (Ti-ERGC, Nikon) and simultaneous bright field time-lapse imaging (iXON 897, Andor Technology). Fig. 2 depicts the details of the MEA-PDMS microchannel device and its mounting onto the microscope stage being equipped with the LMD setup

Table 1 Dissection, activity recording, imaging and medium exchange timeline

| Recording sessions (DIVs and hours) | 17 base | D1 | 17 1h | 17 5h | 18 | 19 | 20 | 21 | 22 | 23 | 24 base | D2 | 24 1h | 24 5h | 25 | 26 | 27 | 28 | 29 | 30 | 31 | 32 | 34 | 36 | 38 | 40 | 42 | 45 |
|---|---|---|---|---|---|---|---|---|---|---|---|---|---|---|---|---|---|---|---|---|---|---|---|---|---|---|---|---|
| Medium exchange | | | | | | | | | * | | | | | | | | * | | | | | * | | * | | * | | * |
| Imaging | * | | * | | * | * | * | * | | * | * | | | | * | * | | * | | * | | | * | * | | * | | * |
| Time spans | 17 | 17d_D1 | | | 18d-24d | | | | | | | 24d_D2 | | | 25d-32d | | | | | | | | 34d-45d | | | | | |

The first row lists the recorded DIVs and highlights the first (orange) and the second (green) dissections. At each dissection DIV, three activity recordings were acquired: baseline (17 base and 24 base), within the first hour after dissection (17 1 h and 24 1 h) and three to five hours after dissection (17 5 h and 24 5 h). Culture medium exchange and bright field imaging days are indicated in the second and third rows. For some analyses, the recorded data for different sessions and DIVs were merged and categorized as time spans as indicated in the last row.



(see also Movie S1‡ with a 3D animation of the setup assembly). All dissection and imaging experiments were performed at room temperature (RT) within 10 min using a 20× objective (CFI Plan Apo VC 20× Air 0.75NA, Nikon). Only the axons in the microchannels with working stations (μ-ch_ws) were dissected in the central working station located 400 μm from both channel ends. Three different dissection levels were applied to three different μ-ch_ws microchannels of each culture at 17 DIV. A complete axonal dissection was induced by passing the focused laser spot (Ø 600 nm) twice across the central working station. Partial dissection was induced by cutting the axons only along half the width of a working station and leaving the remaining axons intact. One week later at 24 DIV, the remaining axonal branches in the other half of the working station were dissected. A local spot dissection was induced by cutting a few axonal branches at one edge of the working station at 17 DIV. One week later at 24 DIV, a partial dissection was performed on the same side of the same axonal bundle.

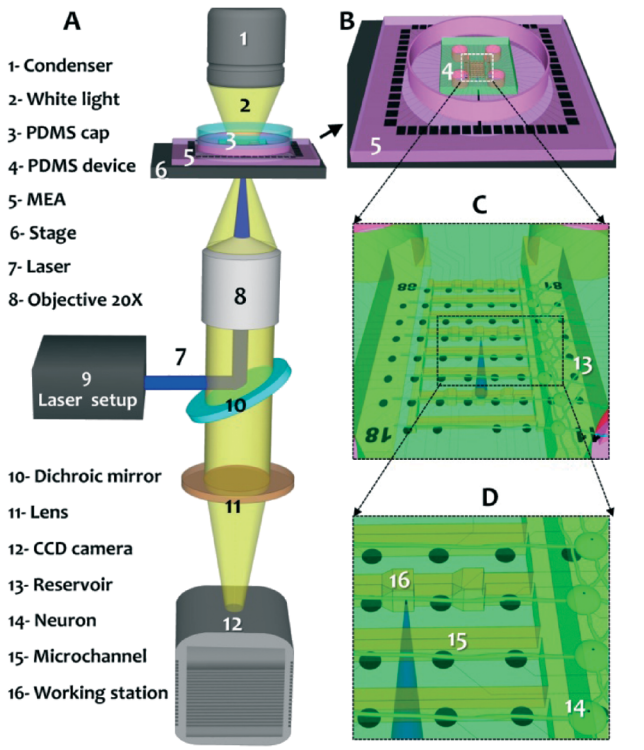


Fig. 2 Laser microdissection system for the selective lesioning of microchannel-confined axons on MEAs. A) Laser and white light path in the assembled setup. White light passes the PDMS cap, PDMS device, neural tissue, MEA substrate, objective, dichroic mirror and lens to image the axons with a CCD camera. Pulsed picosecond UV (355 nm) laser light is reflected by a dichroic mirror and focused onto the axon by a 20× objective. This objective served both for the ablation and the time-lapse imaging. B) The MEA-PDMS assembly was mounted on the motorized stage of the microscope. C) Magnified view of the reservoir, the 8 microchannels and the 8 × 8 electrode matrix. (Composite numbers in the four corners indicate electrode row, then column.) D) Magnified view of the focused laser light (blue cone), MEA electrodes, axons and two microchannel working stations.

The microchannels were selected randomly in each culture to administer complete, partial–partial or local–partial dissections. The network morphology and activity were monitored and recorded at different instances before and after the laser microdissection (Table 1). The control cultures were kept for 10 minutes on the same microscopy stage to record their activity or image their morphology at the same DIVs and times.

### Immunofluorescence staining

Selected cultures were fixed with 4% paraformaldehyde (PFA) and 4% sucrose solution after draining the cell culture medium and washing with warmed 1% PBS. Cell membranes were permeabilized with 0.2% Triton X-100 in 1% PBS for 10 min and incubated with a blocking buffer (2% goat serum (GS) and 3% bovine serum albumin (BSA) in PBS) for 30–45 min. Cultures were incubated with primary antibodies for 3 h at RT, washed 3 times with 1% PBS, then incubated with secondary antibodies for 1 h at RT. The primary antibodies were an anti-rabbit β-tubulin III IgG (SAB4300623, Sigma), anti-rabbit MAP2 IgG (M3696, Sigma) and a mouse monoclonal antibody against the pan-axonal neurofilament (SMI-312R, BioLegend). The secondary antibodies were Alexa Fluor 488 (goat anti-mouse) and 633 (goat anti-rabbit) both from Molecular Probes. Finally, a mounting solution including DAPI to stain the nuclei was added to each culture and covered by a coverslip. Fluorescence was observed using either an upright fluorescence microscope (BX51, Olympus) or an inverted

confocal microscope (TCS SP5 AOBS, Leica). Images were taken by an Optronics Microfire microscope camera (2-megapixel, MBF) and processed with the Neurolucida software package (V1, MBF).

### Statistical analysis

In each hippocampal or cortical culture, the neural activity was recorded by 46 electrodes, 14 of them being located in the reservoir (somata) and 32 underneath the 8 microchannels. The remaining 13 electrodes in the counterpart reservoir did not detect signals and were therefore excluded from analysis. In each microchannel, four subsequent electrodes recorded activity propagation in the same axonal bundle at different positions, two of them proximal to the dissection point and the other two distal thereto. Depending on its relative position within the network, an electrode was placed in one of the following compartment categories: reservoir (somata), control microchannels (intact axons), and completely, partially and locally dissected axons in the proximal and distal sections relative to the injury. Because of the natural fluctuations in the network activity over time and of the different activity levels between cultures on the same day, we treated the spike frequency data from each individual electrode in two different ways before their averaging for each compartment and day or time span, respectively. In method A, the spike frequency (activity) on each electrode was normalized to the maximum activity on one of the MEA electrodes in that recording session before subtracting the electrode-specific baseline activity (normalized pre-dissection activity at 17 DIV). In method B, the percentage of an activity decrease or increase was calculated for defined time spans. Details on the step-by-step analysis are summarized in Table S1.†

Because the spike frequencies were calculated for different groups (dissection *vs.* control) over time, we performed a two-way analysis of variance (ANOVA) with repeated measures in one factor (mixed ANOVA) to allow for 'between group' or 'in group' comparisons over the entire experiment. The resulting data were compared between different time points in the same compartment by repeated measure ANOVA based on estimated marginal means and multiple comparison adjustments by Bonferroni. The mixed ANOVA was followed by *post hoc* Tukey's range test to identify 'between group' differences at specific time points.[28] The data were expressed as the mean ± standard error of the mean (SEM). $p < 0.05$ was considered to be significant.

## Results

We identified the following microchannel design and optimization criteria to study functional regeneration in neural networks after selective laser ablation of axonal projections: the PDMS device had to 1) be transparent to visualize axonal morphology during the transection and its de- or regeneration thereafter; 2) provide a stable microenvironment for long-term cell survival and electrophysiological studies after injury; 3) amplify extracellular activity in somal and axonal compartments to recordable levels, 4) warrant that axonal transection in one microchannel will not physically affect the control axons in the adjacent microchannels; 5) allow for axonal branching and infliction of partial damage to axonal bundles; 6) be compatible with commercial MEA electrode matrix configurations and 7) allow for the independent functional analysis in compartmentalized network architectures including somata, dissected axons and intact axons.

The reported PDMS microchannel device featured microchannels for separating axons from somata and dendrites, for guiding axons and for amplifying extracellularly recorded signals therefrom (Fig. 3A and 4). Closed somal reservoirs provided a stable cellular microenvironment for long-term neuronal network survival and electrophysiology (Fig. 3 and 4). Working stations with extended areas stimulated axonal branching (Fig. 3B, 4D and S2D‡), thereby making them available either for imaging or for focal dissection without affecting other axonal branches in the same working station (Movie S4,‡ and Fig. 3B and S2D‡). Neurite cavities prevented any other cellular compartments (somata, dendrites) but pure, low-density axonal tissue from growing inside the microchannels (Fig. 3C and S2B‡).

By combining such thin PDMS microchannel devices (thickness $< 200$ μm) with commercial glass MEAs, the architecture of neuronal networks could be documented and manipulated by upright or inverted bight-field microscopy (Fig. 4) while simultaneously dissecting the axonal branches and sampling their electrophysiology (see the Movies in the ESI‡). Cortical or hippocampal networks (<3500 neurons per device), either grown in the control groups or in cultures which experienced different types of axonal dissection at different days (17 DIV and 24 DIV), remained functionally alive for 45 DIV. This was a sufficient time to study the effect of axonal injury on network morphology and activity for several weeks after dissection.

### Axonal morphology and activity amplification in the microchannel devices

In all cultures, neurites started to grow homogeneously into the neurite filtering area after 3 DIV and reached the proximal electrodes at the microchannel entries. Within one week, axons had filled all the microchannels and reached the counterpart reservoir (Fig. 4B and D). Each microchannel guided the axons over four subsequent electrodes. In all the cases, the axons tended to grow in axonal assemblies, which we named axonal bundles (Fig. 4B and D and Movie S2‡). However, upon their entrance into the wider areas of the working stations or the distal reservoir, these bundles branched out to distribute their individual axons over the entire width (Fig. 3 and S2‡).

In almost all networks, the first signals were recorded at 7 DIV from axons on the electrodes inside the microchannels, but not from the electrodes in the quasi-closed somal reservoirs. Therein, network activity appeared around 10 DIV at the earliest. In contrast, in predecessor devices with open

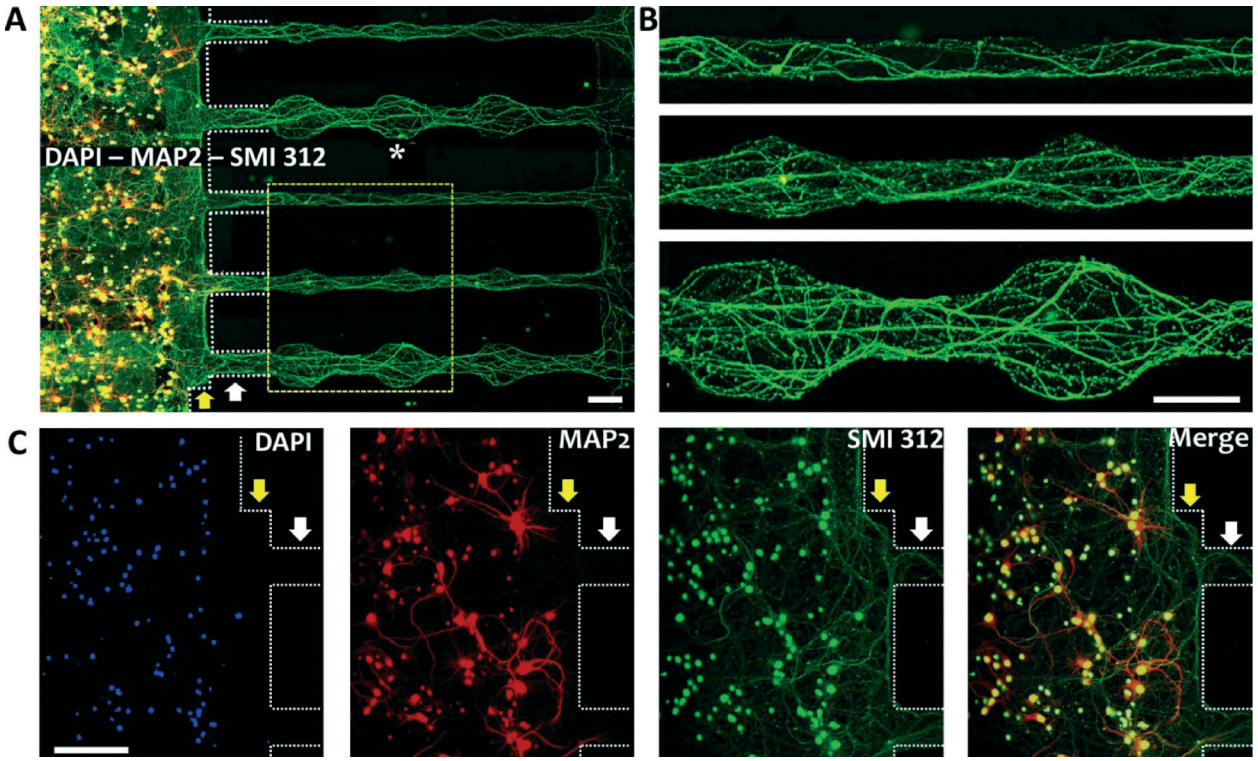


**Fig. 3** Immunofluorescence images of cultures on coverslips. A) Merged image of nuclei (DAPI, blue), somata and dendrites (MAP2, red), and axons (SMI 312, green) from five microchannels (white arrow), the somal reservoir (left), the neurite cavity (yellow arrow) and the axonal compartment (right). The white asterisk points to one of the six visible working stations (extended area in a μ-ch_ws). The white dashed line represents the border between reservoir, neurite cavity and microchannels. B) Magnified view (yellow rectangle in A) of the axonal morphology in the different microchannel types. The bottom panel shows axonal branching in the two working stations of a μ-ch_ws. C) Nuclei (DAPI, blue), somata and dendrites (MAP2, red), axons (SMI 312, green) and merged images of an area including the reservoir, the neurite cavity (yellow arrow) and the proximal section of two microchannels (white arrow). Scale bars: 50 μm.

somal reservoirs in direct contact with the bulk medium above, only a few electrodes recorded activity at very late DIVs (data are not shown). The average signal amplitude on the electrodes recording from axons inside the microchannels was twice that of the somata in the closed chambers (400 μV *vs.* 200 μV with a maximum amplitude of 1.2 mV *vs.* 400 μV). Recorded signals from the subsequent electrodes inside the microchannels confirmed directional activity propagation including bursts and single spikes (Fig. 4C).

With the exception of the working stations, the width of both uniform microchannels and of the microchannels with working stations was identical (30 μm). To explore whether local changes in microchannel geometry alter the biophysical properties of the recorded signals, we compared the spike rate in μ-ch_ws with that in straight μ-ch in hippocampal control cultures. As depicted in Fig. S1C and S1D,‡ no significant differences in the spike amplitudes and mean frequencies could be found.

### Axonal morphology and activity after dissection

Although the focusing and positioning of a laser dissection beam within a μ-ch is a relatively easy and common task, the reproducible and controllable ablation of an axonal bundle from partial to complete dissection is not trivial. Laser ablation predominantly occurs through the cavitation and collapse of a microbubble followed by the emission of a pressure shock wave (Movie S2‡). In slim microchannels, the laser-induced pressure shock wave usually propagates and reaches the PDMS walls quickly. This results in the formation of a larger cavitation bubble and its less confined disruption within the channel itself.[39] In order to reduce such unwanted side effect, broader microchannels are preferable. However, geometrical constraints impose a certain width to obtain an efficient separation of axons from their somata (see the Methods section). We found a good compromise by introducing enlarged working stations while maintaining reduced microchannel widths along the remaining microchannel length. This provided the required volume for the precise laser dissection of individual axons. The maximal width of a working station is only limited by its width-to-height ratio to avoid the collapse of the microchannel roof. Moreover, the working stations induced the branching of axonal bundles and thereby allowed to selectively inflict a local or partial damage to only a few of the many branches (μ-ch_ws; Movies S4 and S5‡). In contrast, a partial dissection in non-separated axonal assemblies growing inside a microchannel without working station (μ-ch) actually severed all axonal fibers in a

 

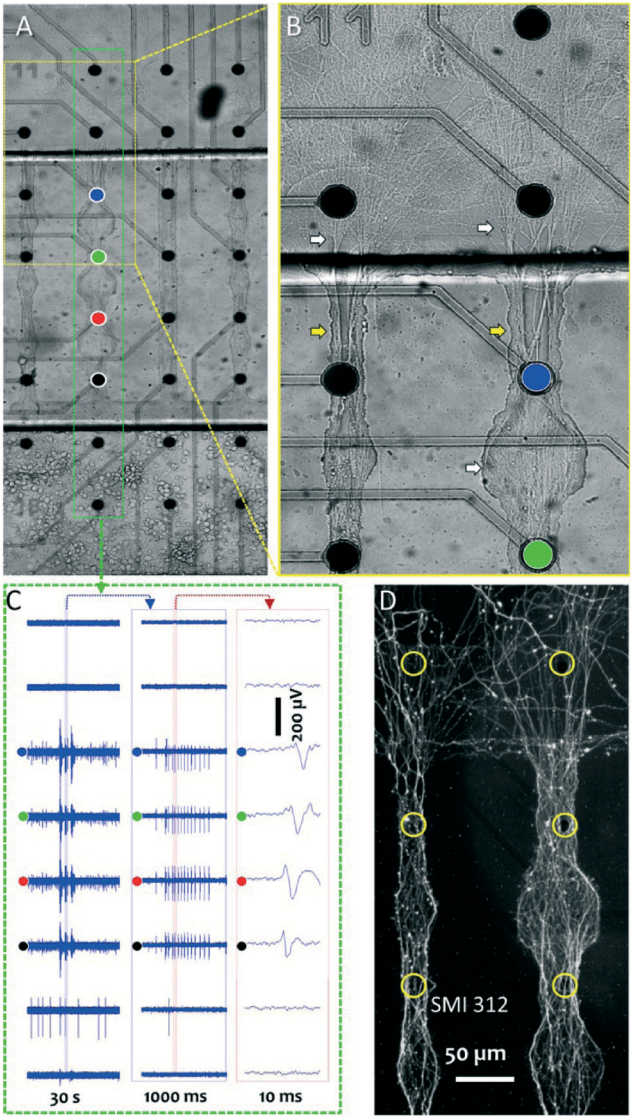


**Fig. 4** Sample morphology and recording from cortical neurons in the μ-ch_ws devices. A) Cortical culture at 16 DIV. Four subsequent electrodes recorded from the same axon assembly at different positions in each microchannel (colored circles; black, red, green, blue). B) Magnified view of the yellow region in A showing axonal bundles in the narrow sections (yellow arrows) and branched axons in the wider areas (axonal reservoir and working stations; white arrows). C) Recording profile from the 8 electrodes inside the green frame in A, out of which four were recording from the axonal bundles inside the microchannel (colored circles in A). All three columns show the same recordings at different temporal resolutions: propagation of spike assemblies (burst activity; left), zoom into one of the bursts (middle) and propagation of a single spike along the axon (right). D) Fluorescence microscopy image from the axons growing inside a μ-ch (left) and μ-ch_ws (right) on a MEA. Axonal branches were labeled by SMI 312. Yellow circles denote the positions of the recording electrodes.

bundle including the axons on the opposite edge of the same microchannel. This was a consequence of the above described mechanical shear stress associated with the formation and expansion of laser-induced cavitation bubbles (Movie S2‡).

At 17 DIV, a complete axonal dissection in a working station created a gap between detached distal and proximal axons (Fig. 5C). Visually, degeneration was not obvious right after dissection. However, within one week, disconnected distal axonal bundles inside the microchannel and at the exit point to the opposite reservoir showed signs of progressive anterograde degeneration including axonal beads and fragments (Fig. 5D). Dissecting an entire axonal bundle in one microchannel did not directly affect the axons in the adjacent microchannels (Fig. S3‡). Furthermore, signals could still be detected by the first distal electrode close to the dissection point, although with decreased amplitude and frequency. Activity in the distal section recovered in the subsequent weeks (Fig. 5E).

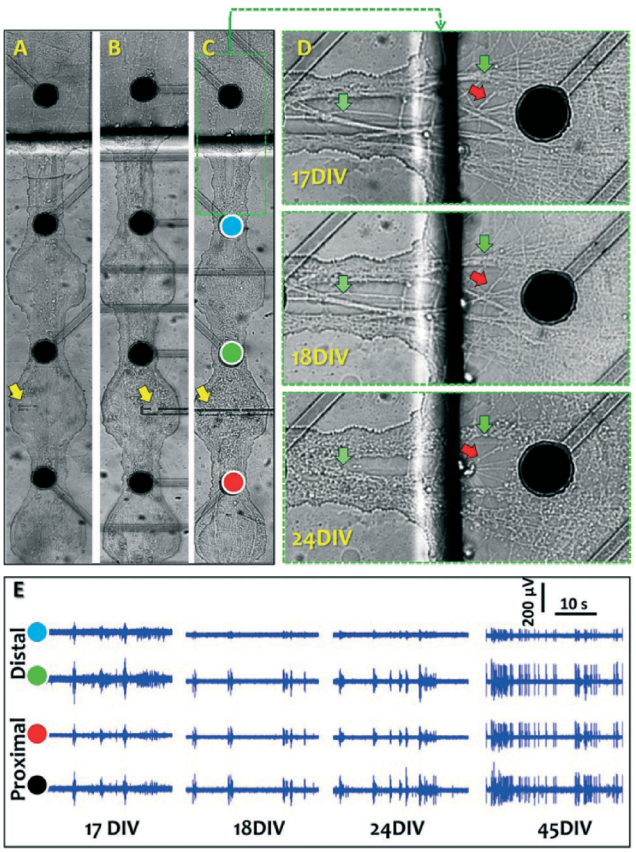


**Fig. 5** Sample axonal morphology and activity after axonal dissection. A) Axonal morphology one week after the first local dissection at 17 DIV (Movie S5‡). B) Axonal morphology one week after the first partial dissection at 17 DIV (Movie S4‡). C) Axonal morphology one week after a complete dissection at 17 DIV (Movie S3‡). The laser line signature in the middle of each working station (A–C) marks the dissection path (yellow arrows). D) Zoom onto the morphology in the rectangular area outlined in green in C before (top, 17 DIV), one day (middle, 18 DIV) and one week (bottom, 24 DIV) after the complete dissection of confluent axonal bundles in a cortical culture. Green arrows indicate degenerating axons, red arrows intact or regenerating axons. E) Recorded activity profile of a completely dissected axonal bundle on two proximal (black and red disks) and two distal electrodes (green and blue disks) at different days. The most proximal electrode (black circle) is not visible in C.

A partial dissection within a working station at 17 DIV physically disconnected the proximal and distal parts of an axon assembly, whereas the rest of the branched-out axons in the non-dissected areas of the same microchannel remained intact (Fig. 5B and Movie S4‡). After completing the dissection at 24 DIV, the number of degenerating distal axons increased more dramatically when compared to the first partial dissection at 17 DIV (Fig. S4‡).

A focal dissection of a few axonal branches in a big confluent axonal bundle led to the degeneration of the dissociated distal axonal fragments on the subsequent DIVs while the rest of the axonal projections in the same bundle remained intact (Fig. 5A). A partial dissection of the same axonal bundle 7 DIVs later (24 DIV) led to degeneration signs in most axons entering the opposite reservoir at subsequent DIVs. A qualitative comparison of a partial dissection at 24 DIV with the one at 17 DIV showed that partial axonal injury at 17 DIV was less deteriorative than at 24 DIV.

For all the dissection types, degenerating distal axons remained attached to the MEA substrate in both the microchannels and inside the reservoir for 4 subsequent weeks. This helped in visualizing progressive axonal degeneration over time (Fig. 5 and S3‡).

### Functional response to axonal dissection

Spike frequency (SF; spikes per second) was used as an index for neuronal activity and function. Different electrodes were recording from different parts of the network. For easier comparison, we functionally separated each network into the following modules: reservoir (somata), intact axons, completely dissected axons, partially dissected axons, and locally dissected axons. All axonal activities were further compartmentalized into proximal and distal sections (Fig. 6 and 7, Table S1‡). We performed two types of analyses on the spike frequency data (Table S1‡). The first method (A; normalized

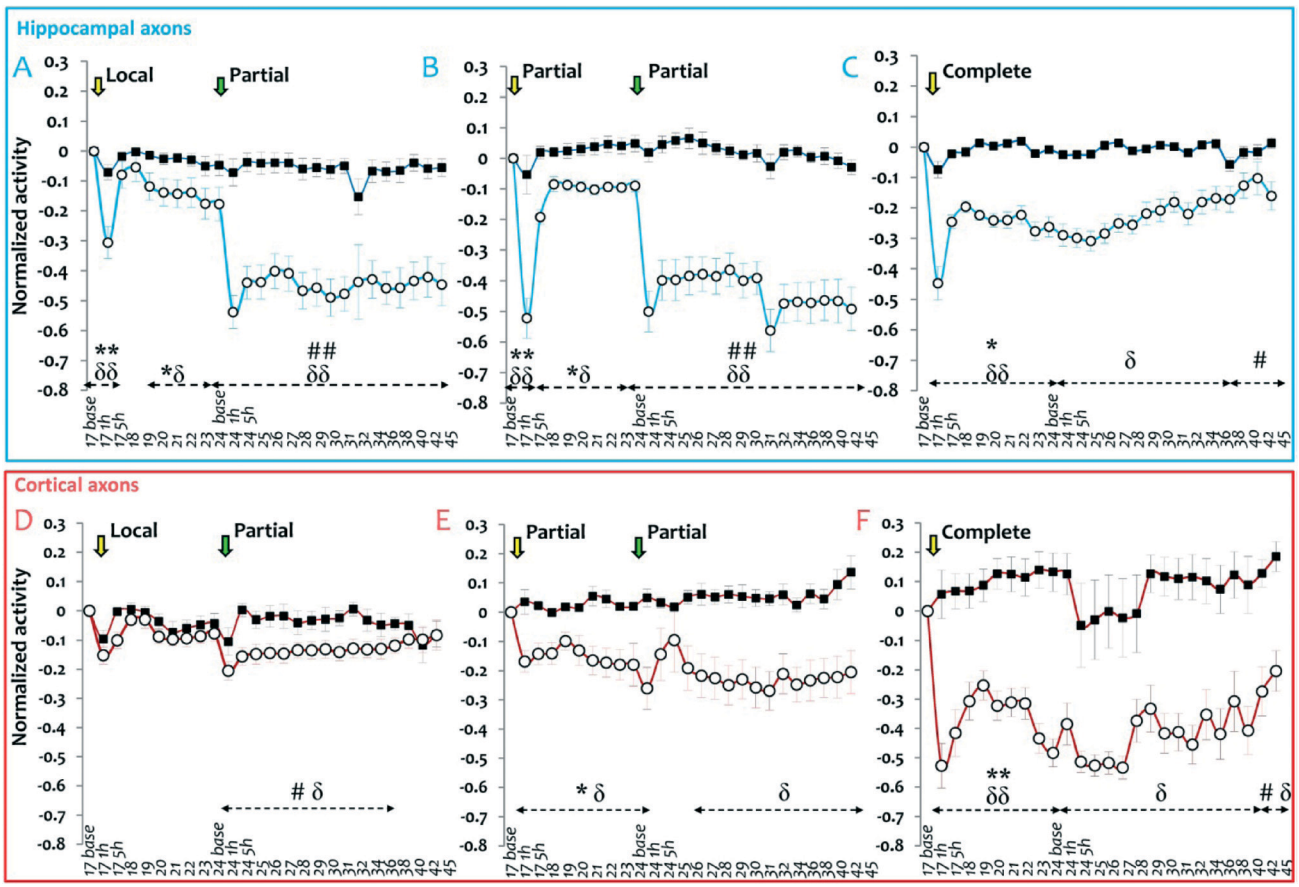


**Fig. 6** Normalized activity of dissected hippocampal and cortical axons. At each dissection DIV, activity was recorded three times: at baseline (17 base and 24 base), just after dissection (17 1 h and 24 1 h) and three to five hours after dissection (17 5 h and 24 5 h). The first and second dissections (17 DIV and 24 DIV) are represented by yellow and green arrows, respectively. Plots of the baseline-corrected, maximum-normalized and averaged activity in the proximal *vs.* distal parts of locally (A), partially (B) and completely (C) dissected hippocampal axons as well as locally (D), partially (E) and completely (F) dissected cortical axons. Proximal and distal axons are represented by squares and circles, respectively. Results are given as the means ± SEM. A mixed ANOVA followed by *post hoc* Tukey's test was applied to compare the mean difference between activity in the proximal and distal sections ($\delta$ $p < 0.05$ and $\delta\delta$ $p < 0.01$). A repeated measure ANOVA was applied to compare the post-dissection activity with the pre-dissection baseline activity before the first and the second dissections (* $p < 0.05$, ** $p < 0.01$ *vs.* 17 base and # $p < 0.05$ and ## $p < 0.01$ *vs.* 24 base).

 

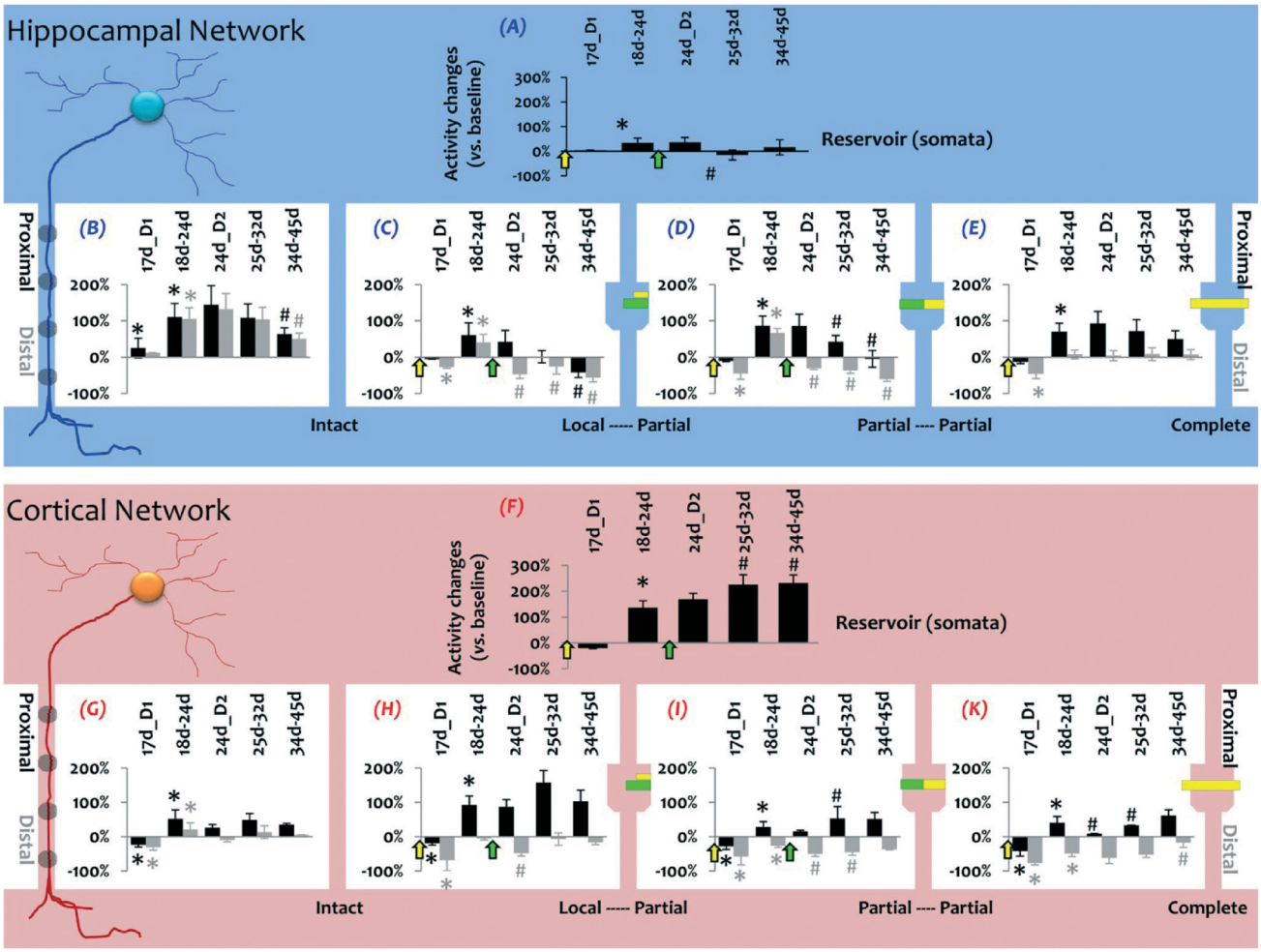


Fig. 7 Activity change in each compartment after selected axonal dissection. Summary of activity changes (percentage) *vs.* pre-dissection baseline (17 base) in all three recording compartments (somal reservoir, proximal and distal to the injury) pooled from all MEAs (hippocampal: $n$ = 6, A–E, and cortical: $n$ = 5, F–K) in (A, F) the somal reservoir, (B, G) in control microchannels, (C, H) for locally (17 DIV) and partially (24 DIV) dissected axonal bundles, (D, I) for twice partially dissected axonal bundles (17 DIV and 24 DIV) and (E, K) for completely dissected axonal bundles (17 DIV). To simplify the analysis, the data from different sessions and DIVs were merged within the time spans defined in Table 1. The data from the somal and proximal axons are plotted with black bars, the data from distal axons with gray bars. The results are given as the means ± SEM for each time span. In each group, the mean activity for the different time spans was compared by repeated measure ANOVA. * $p < 0.05$ compares the activity in the week after the first dissection with the pre-dissection activity at 17 DIV. # $p < 0.05$ compares the activity in the weeks after the second dissection with that over the time span between 18 DIV and 24 DIV.

activity) normalized the data recorded from all electrodes on each MEA to the maximum activity on that MEA in each recording session. Since the activity levels varied between cultures, normalization cancelled out any difference between cultures at each time point (Fig. 6). The second method (B; activity change) calculated the percentage activity increase or decrease with respect to the pre-dissection values at 17 DIV for all DIVs in each compartment. Since the baseline activity differed between compartments, this method neutralized its effect (Fig. 7).

The normalized data showed a slight activity reduction in the distally disconnected axons after local or partial dissections at 17 DIV (Fig. 6A, B and D, E). It was followed by further activity loss after a second partial dissection at 24 DIV (Fig. 6A, B and D, E). The activity did not recover after a complete dissection at 17 DIV, though (Fig. 6C and F). For both cell types, the distal activity decrease in the dissected axons reflected the degree of inflicted damage at 17 DIV (Fig. 6). Subsequent partial dissections of the same axonal bundles (17 DIV and 24 DIV) led to a step-wise activity reduction in the distal hippocampal or cortical axonal fragments (Fig. 6A, B and D, E).

The main observed differences between the cortical and hippocampal neurons can be summarized as follows. Somata: cortical cultures showed a consistent activity increase after both the first (17 DIV) and the second (24 DIV) dissections ($p < 0.05$; Fig. 7F), whereas the activity in the hippocampal cultures increased only after the first dissection, but decreased after the second dissection ($p < 0.05$; Fig. 7A). Intact axons: compared to the cortical cultures, intact hippocampal axons were highly active with an early activity onset and a long-lasting response after both dissections ($p < 0.05$;

Fig. 7B and G). Instead, intact cortical axons showed increased activity only after the first dissection with a late onset (Fig. 7G). Distal axonal segments (dissected at 17 DIV): the activity of the distal hippocampal axonal segments recovered faster (>20%, within 5 h; Fig. 6A–C) compared to the distal cortical axonal segments (>20%, within 2 DIVs; Fig. 6D–F) after a local, partial or complete dissection at 17 DIV (Fig. 7). Distal axonal segments (dissected at 24 DIV): partial dissection at 24 DIV resulted in a more dramatic activity decrease in the distal hippocampal axonal segments when compared to the cortical axons (Fig. 6A, B, and D, E). While the activity recovered in the distal cortical axonal segments during the subsequent weeks, it remained at lower levels in the distal hippocampal axonal fragments (Fig. 7C, D and H, I). Proximal axon stumps: after the first dissection at 17 DIV, the axonal activity increased in both cell types proximal to the location of the injury ($p < 0.05$; Fig. 7C, D and H, I). However, after the second dissection at 24 DIV, the activity decreased in the proximal hippocampal axon stump (Fig. 7C and D), whereas it gradually increased in the proximal cortical axon stump (Fig. 7H, I).

# Discussion

Almost all previous studies on axonal injury using suction or laser microdissection in random cultures or in microfluidic devices focused on axonal biology and structural changes rather than axonal electrophysiology or functional response to a focal injury.[10,12–14,29,30] To the best of our knowledge, this is the first report on the functional network response to a tunable axonal dissection by combining MEA technology with UV-LMD-optimized microchannel devices over time spans of more than 6 weeks. The separation of somata and dendrites from axons through neurite cavities and the selective microchannel-confinement of axons to the recording electrodes of MEAs served several purposes. Neurite cavities limited the presence of the somata and dendrites to the proximal sections of the microchannels without allowing them to penetrate into the microchannels. In addition, they decreased the number of axons growing into the microchannels, thereby facilitating imaging and axonal dissection. Furthermore, the microchannels not only amplified the extracellularly recorded signals, but allowed us to locally monitor the activity dynamics in different network compartments as well as in different sections of both intact and dissected axons. Device transparency and geometries (*i.e.* the inclusion of working stations) enhanced the optical access for the laser manipulation and the imaging of individually identifiable axonal branches.

### PDMS devices optimized for MEA electrophysiology

In preliminary designs, we considered PDMS microchannel devices with open reservoirs similar to the designs being used for MEA electrophysiology by other groups.[19,20] Even though we could capture extracellular activity from microchannel-confined axons, that of the corresponding small neuronal network located in an open reservoir was rarely visible (data not shown). To improve the signal quality in the reservoirs, we therefore sealed them from the top by a simple modification of the PDMS molding procedure (Fig. 1A). These quasi-closed somal reservoirs were connected to rather large open cavities ($r$ = 1 mm) by tiny gates (100 μm × 200 μm; Fig. 1C), which dampened any changes in the bulk cell culture medium outside of the reservoirs. They thereby prevented rapid changes in the pH and attenuated mechanical and biochemical disturbances of the local microenvironment. These usually result from handling artifacts during recording, microscopy and experimental interventions including medium exchange. This physical separation is advantageous for electrophysiology because network activity is prone to modulation by even slight fluctuations in the culture environment, which can dramatically affect the results of an experiment.[26,31–34]

Furthermore, to reduce network complexity and to place the majority of somata onto or nearby the available electrodes, the reservoirs featured very small dimensions (0.4 × 1.6 $mm^2$) compared to previously reported models.[20] This microchannel tile design allowed us to keep small-world cortical or hippocampal networks (<3500 neurons per device) functionally alive for more than 6 weeks. Previous studies confirm the difficulty of sustaining the viability of low-density networks over such long periods.[35] In most cases, it was therefore problematic to collect sufficiently large activity datasets for analyzing functional network properties.[36,37] However, there is great potential in exploiting such small long-living networks with rich activity for different experimental purposes (*e.g.* chronic effect of drug treatment, axonal regeneration and plasticity).

The presented device was designed for commercial MEAs with an 8 × 8 electrode matrix layout, an electrode pitch of 200 μm and an overall edge length of 20 mm. Its microchannel configuration could be easily adapted to other electrode configurations or electrode pitches. The current microchannel width is less than 35 μm. It therefore covers already the entire range of the electrode diameters (10–30 μm) of currently available MEAs. The overall device dimensions should stay below 24 × 24 $mm^2$ to fit on MEAs with different inner ring diameters (24 mm to 30 mm).

### PDMS devices optimized for selective axonal laser microdissection

The physical dimensions of the microchannels allow them to host both axons and dendrites. Therefore, despite the more rapid and longer axonal growth, the proximal parts of the microchannels always contain some percentage of dendrites mixed with the axonal branches.[12] To prevent dendrite growth into the microchannels and to thus let only pure axonal branches populate the proximal microchannels, we added a low-profile neurite filtering area between the reservoir and the microchannels (Fig. 1C, 3C and S2‡). The neurite filtering area also decreased the axonal density inside a microchannel

 

and thus facilitated the imaging of the individually identifiable axons. Furthermore, microchannels isolated axonal bundles from each other, which allows studying focal axonal damage in a selected microchannel without directly affecting the axons in the adjacent microchannels.

In the straight microchannels without lateral expansions, the axons tended to form big bundles or fascicles and thus made it difficult to inflict a partial or very local damage to a few axonal branches only (Movie S2‡). In addition, morphological changes in the composition of the axonal branches were not clearly visible. Previous studies reported that axonal bundles branched at the microchannel exit, thereby separating individual axons from each other.[38] We translated this concept by adding extended areas, so-called working stations, along three microchannels in each device (Fig. 1C). As a result, the axonal bundles already branched within the working stations (Fig. 3B and S2D‡). Thus, the axonal morphology could be monitored more easily, and individual axons became available for partial or local transection (Fig. 5B and C and Movies S4 and S5‡). This strategy also allowed for repeating or concluding a dissection on the same axonal bundle at any later time.

Picosecond pulsed UV lasers induce cell lysis by plasma formation and cavitation bubble expansion or collapse.[39,40] Because these processes are difficult to control, we observed cavitation bubble expansion over the entire width of a straight microchannel (μ-ch; Movie S2‡). This not only led to the complete dissection of an axonal bundle along one edge of a microchannel, but mechanically affected also a separate axonal bundle growing along the opposite edge of the same microchannel. In contrast, cavitation bubbles that formed in the wider areas of the microchannel working stations tended to be smaller, thereby inflicting more localized damage to a few axonal branches only while leaving others intact (Movies S4 and S5‡). This geometry-assisted fine-control is reflected by the stepwise activity decrease and partial recovery in the subsequently dissected axons at 17 DIV and 24 DIV (Fig. 6A, B and D, E).

Because the device is thin (200 μm), dissection can theoretically be performed both in upright and inverted microscopy setups, and allows for the use of short working distance objectives.

### Distal axon degeneration after axotomy

After complete dissections, the distal axonal fragments experienced progressive anterograde degeneration that started soon after surgery and progressed over the four subsequent weeks (Fig. 5D). The morphological changes and their evolution in these distal sections showed strong similarities to Wallerian degeneration.[15,41] It occurs within 24 h hours after PNS or CNS axonal injury in the axonal sections distal to the injury and includes axonal fragmentation and swelling.[42] Usually, degenerating distal sections on coverslips or glass slides detach from the substrate after three days at the latest, though, which makes it impossible to study distal degeneration phenomena on later days.[14]

In contrast, we observed that degenerating distal axons remained attached to the MEA surface inside or outside of the microchannels up to the end of the study at 45 DIV (Fig. 5D and S3‡). This finding suggests a stronger adhesion of the axonal membrane to the MEA substrate if compared to the glass slides. This could be related to the silicon nitride ($Si_3N_4$) insulation layer, its topology or to the altered, more favorable surface chemistry after its oxygen plasma treatment that preceded the coating with PDL and laminin. Regardless of the cause that kept degenerating axons attached to the substrate, this feature could be exploited in other *in vitro* models of axonal degeneration.[2,15]

Despite the significant activity decrease in the distal segments of the completely dissected axons, the activity did not disappear on the first distal electrode, neither during the first few hours after dissection nor at later days (Fig. 5E). This could have different reasons. Firstly, *in vivo*, detached distal axons preserve their excitability for days after dissection and are able to conduct action potentials if stimulated.[43,44] Secondly, the gap size between the proximal and distal axonal segments is a decisive factor in axonal repair after dissection.[45] It has been shown that nerves can reconnect over dissection gaps of less than 4 cm.[46]

### Partial and stepwise dissections on selected axonal bundles

Different dissection levels in the same cortical or hippocampal culture led to different axonal activities in distal sections depending on the severity of the damage (Fig. 6). In previous studies, the laser power had to be adjusted very precisely to inflict partial damage to a few axons inside a big confluent bundle.[14] In our model, axonal branches self-detangled automatically in the working stations. This allowed us to simply cut a few branches while leaving other axons intact (Movie S4‡). Our approach furthermore allowed for the stepwise induction of a desired axonal damage at different days, as the gradual activity decrease after the first and the second local or partial axonal dissections in the cortical and hippocampal cultures exemplified (Fig. 6A, B and 6D, E).

Despite the activity loss in the distal axonal segments, the activity increased in the proximal segments after the first dissection in both the proximal membrane and in the regenerating portion of the axons in the subsequent days, which increases membrane excitability.[30,44]

### Cell type-dependent discrepancy in response to axonal dissection

Cortical and hippocampal network activity increased in response to a dissection at 17 DIV and remained high during the subsequent week. Such activity increase after axotomy had already been observed in cultured hippocampal neurons at a younger age.[30] However, after the second dissection at 24 DIV, the cortical network activity remained stable, whereas the activity decreased in the hippocampal cultures (Fig. 7A and F). This could be related to the intrinsic difference between the two neural types, which suggests that the hippocampal

neurons are more susceptible to stress compared to the cortical neurons. For instance, oxygen and glucose deprivation in hippocampal neurons increased the AMPA receptor (AMPAR) subunit GluA2 endocytosis, which is absent in cortical neurons.[47]

Conversely, the distal hippocampal axon segments showed faster activity recovery after dissection at 17 DIV. It has been shown that in response to the same mechanical stress *in vitro*, cortical neurons respond with mild but longer increase in intracellular free calcium concentration ($Ca^{2+}$), whereas hippocampal neurons respond with a large and fast increase in intracellular $Ca^{2+}$.[48] In addition, ATP deficits already appear within 1 h after mechanical stress in cortical neurons, but only after 24 h in hippocampal neurons.[48]

To start with a rich network activity and to make our *in vitro* model more similar to axonal degeneration in the adult brain, our dissections were carried out on older than ever reported primary cortical and hippocampal neurons at 17 DIV and 24 DIV. Most of the previous *in vitro* axonal dissection studies were performed on younger cultures between 3 DIV and 10 DIV and mainly on individual axonal branches. However, it has been shown that network activity in terms of spike frequency increases between 14 DIV and 17 DIV in both cortical and hippocampal cultures. It reaches a stable state after the complete maturation of excitatory connections at 21 DIV.[36,49] This natural evolution of network dynamics in cultured hippocampal and cortical neurons therefore helped us in studying the effect of axonal injury on network dynamics and axonal electrophysiology for two maturation stages with different activity levels, rich or increasing activity after the first dissection at 17 DIV and stable or decreasing activity after the second dissection at 24 DIV (Fig. S1‡).

## Conclusion

The presented MEA-LMD-microchannel setup permitted network compartmentalization into structural and functional modules including somata, intact axons as well as proximal and distal segments of dissected axons. In addition, the controlled axonal dissection in one specific module could be carried out without affecting the network compartments in the other modules. Beyond being precise in inflicting a focal and stepwise axonal injury, the device provided other advantages like long-term culture survival and improved signal quality recorded from both axons and somata. This allowed us to comparatively study proximal and distal axonal degeneration and functional response by optical and electrophysiological means. Besides the possibility of investigating network activity in more detail, the combination of electrophysiology with the other experimental approaches including morphological, molecular, optogenetic and pharmacological tools may lead to a better understanding of the mechanisms involved in neural plasticity, network dynamics after injury and axonal de- or regeneration.

## Acknowledgements

We would like to thank Marina Nanni for her assistance in the cell culture preparation and for microfabrication support from the cleanroom team. IIT intramural funds in support of this research are highly appreciated.

## References

1 D. Debanne, *Nat. Rev. Neurosci.*, 2004, **5**, 304–316.
2 L. Conforti, J. Gilley and M. P. Coleman, *Nat. Rev. Neurosci.*, 2014, **15**, 394–409.
3 H. C. Wang and Y. B. Ma, *J. Clin. Neurosci.*, 2010, **17**, 157–162.
4 M. Abu-Rub, S. McMahon, D. I. Zeugolis, A. Windebank and A. Pandit, *Drug Discovery Today*, 2010, **15**, 436–443.
5 M. F. Yanik, H. Cinar, H. N. Cinar, A. D. Chisholm, Y. S. Jin and A. Ben-Yakar, *Nature*, 2004, **432**, 822–822.
6 S. X. Guo, F. Bourgeois, T. Chokshi, N. J. Durr, M. A. Hilliard, N. Chronis and A. Ben-Yakar, *Nat. Methods*, 2008, **5**, 531–533.
7 C. Balaratnasingam, W. H. Morgan, L. Bass, M. Kang, S. J. Cringle and D. Y. Yu, *Neuroscience*, 2011, **177**, 269–282.
8 N. Hyun, L. Z. Shi and M. W. Berns, *Methods Mol. Biol.*, 2015, **1254**, 211–226.
9 F. Difato, H. Tsushima, M. Pesce, F. Benfenati, A. Blau and E. Chieregatti, *Sci. Rep.*, 2011, **1**, 183.
10 Y. T. Kim, K. Karthikeyan, S. Chirvi and D. P. Dave, *Lab Chip*, 2009, **9**, 2576–2581.
11 A. M. Taylor and N. L. Jeon, *Curr. Opin. Neurobiol.*, 2010, **20**, 640–647.
12 A. M. Taylor, M. Blurton-Jones, S. W. Rhee, D. H. Cribbs, C. W. Cotman and N. L. Jeon, *Nat. Methods*, 2005, **2**, 599–605.
13 J. W. Park, B. Vahidi, A. M. Taylor, S. W. Rhee and N. L. Jeon, *Nat. Protoc.*, 2006, **1**, 2128–2136.
14 A. N. Hellman, B. Vahidi, H. J. Kim, W. Mismar, O. Steward, N. L. Jeon and V. Venugopalan, *Lab Chip*, 2010, **10**, 2083–2092.
15 D. Kilinc, J. M. Peyrin, V. Soubeyre, S. Magnifico, L. Saias, J. L. Viovy and B. Brugg, *Neurotoxic. Res.*, 2011, **19**, 149–161.
16 Y. Nam and B. C. Wheeler, *Crit. Rev. Biomed. Eng.*, 2011, **39**, 45–61.
17 Y. Nam, J. Chang, D. Khatami, G. J. Brewer and B. C. Wheeler, *IEE Proc.: Nanobiotechnol.*, 2004, **151**, 109–115.
18 B. J. Dworak and B. C. Wheeler, *Lab Chip*, 2009, **9**, 404–410.
19 B. C. Wheeler and G. J. Brewer, *Proc. IEEE. Inst. Electr. Electron. Eng.*, 2010, **98**, 398–406.
20 L. B. Pan, S. Alagapan, E. Franca, G. J. Brewer and B. C. Wheeler, *J. Neural. Eng.*, 2011, **8**, 046031.
21 W. Ling, R. Michael, B. Jennifer Olmos and C.-T. Enric, *J. Neural. Eng.*, 2012, **9**, 026010.
22 L. Pan, S. Alagapan, E. Franca, T. DeMarse, G. J. Brewer and B. C. Wheeler, *IEEE Trans. Neural. Syst. Rehabil. Eng.*, 2014, **22**, 453–459.
23 E. Claverol-Tinture, M. Ghirardi, F. Fiumara, X. Rosell and J. Cabestany, *J. Neural. Eng.*, 2005, **2**, L1–7.

 

24 E. Claverol-Tinture, J. Cabestany and X. Rosell, *IEEE Trans. Biomed. Eng.*, 2007, **54**, 331–335.
25 F. Difato, M. Dal Maschio, E. Marconi, G. Ronzitti, A. Maccione, T. Fellin, L. Berdondini, E. Chieregatti, F. Benfenati and A. Blau, *J. Biomed. Opt.*, 2011, **16**, 051306.
26 A. Blau, T. Neumann, C. Ziegler and F. Benfenati, *J. Biosci.*, 2009, **34**, 59–69.
27 F. Difato, L. Schibalsky, F. Benfenati and A. Blau, *Int. J. Optomechatronics*, 2011, **5**, 191–216.
28 A. Field, *Discovering Statistics Using SPSS*, 3rd edn, 2009.
29 H. J. Kim, J. W. Park, J. W. Park, J. H. Byun, B. Vahidi, S. W. Rhee and N. L. Jeon, *Ann. Biomed. Eng.*, 2012, **40**, 1268–1276.
30 C. Tsantoulas, C. Farmer, P. Machado, K. Baba, S. B. McMahon and R. Raouf, *PLoS One*, 2013, 8.
31 S. Halldorsson, E. Lucumi, R. Gomez-Sjoberg and R. M. Fleming, *Biosens. Bioelectron.*, 2015, **63**, 218–231.
32 J. Hogins, D. C. Crawford, C. F. Zorumski and S. Mennerick, *PLoS One*, 2011, **6**, e25633.
33 L. J. Millet and M. U. Gillette, *Trends Neurosci.*, 2012, **35**, 752–761.
34 D. Saalfrank, A. Konduri, S. Latifi, R. Habibey, A. Golabchi, A. Martiniuc, S. Ingebrandt and A. Blau, *R. Soc. Open Sci.*, 2015, **2**, 150031.
35 A. Kaneko and Y. Sankai, *PLoS One*, 2014, **9**(7), e102703.
36 E. Biffi, G. Regalia, A. Menegon, G. Ferrigno and A. Pedrocchi, *PLoS One*, 2013, **8**, e83899.
37 D. Ito, H. Tamate, M. Nagayama, T. Uchida, S. N. Kudoh and K. Gohara, *Neuroscience*, 2010, **171**, 50–61.
38 J. M. Peyrin, B. Deleglise, L. Saias, M. Vignes, P. Gougis, S. Magnifico, S. Betuing, M. Pietri, J. Caboche, P. Vanhoutte, J. L. Viovy and B. Brugg, *Lab Chip*, 2011, **11**, 3663–3673.
39 P. A. Quinto-Su, H. H. Lai, H. H. Yoon, C. E. Sims, N. L. Allbritton and V. Venugopalan, *Lab Chip*, 2008, **8**, 408–414.
40 K. R. Rau, A. Guerra, A. Vogel and V. Venugopalan, *Appl. Phys. Lett.*, 2004, **84**, 2940–2942.
41 S. Rotshenker, *J. Neuroinflammation*, 2011, **8**, 109.
42 A. D. Gaudet, P. G. Popovich and M. S. Ramer, *J. Neuroinflammation*, 2011, **8**, 110.
43 B. Mishra, R. Carson, R. I. Hume and C. A. Collins, *J. Neurosci.*, 2013, **33**, 18728–18739.
44 M. Moldovan, S. Alvarez and C. Krarup, *Brain*, 2009, **132**, 511–523.
45 M. Cho, *Nat. Neurosci.*, 2009, **12**, 1085–1085.
46 C. Krarup, S. J. Archibald and R. D. Madison, *Ann. Neurol.*, 2002, **51**, 69–81.
47 E. Blanco-Suarez and J. G. Hanley, *J. Biol. Chem.*, 2014, **289**, 4644–4651.
48 D. M. Geddes, M. C. LaPlaca and R. S. Cargill 2nd, *Exp. Neurol.*, 2003, **184**, 420–427.
49 M. Chiappalone, M. Bove, A. Vato, M. Tedesco and S. Martinoia, *Brain Res.*, 2006, **1093**, 41–53.